A Series of Dimeric Cobalt Complexes Bridged by N-Heterocyclic Phosphido Ligands.

Andrew M. Poitras,[†] Mark W. Bezpalko,[‡] Curtis E. Moore,[†] Diane A. Dickie,[‡§] Bruce M. Foxman,[‡] and Christine M. Thomas[†]*

[†]Department of Chemistry and Biochemistry, The Ohio State University, 100 West 18th Avenue, Columbus, Ohio, 43210, United States

[‡]Department of Chemistry, Brandeis University, 415 South Street, Waltham, Massachusetts 02454, United States

Supporting Information Placeholder

ABSTRACT: A tridentate [PPP] ligand has been used to construct a series of dimeric cobalt complexes and explore cooperative multielectron redox processes that are both metal- and ligand-centered. Reduction $(PP^{Cl}P)CoCl_2$ (**1**) with excess magnesium affords the $Co^{I}Co^{I}$ *N*-heterocyclic phosphido (NHP^-)-bridged symmetric dimer $[(PPP)Co]_2$ (**2**). Two-electron oxidation of **2** with $FcPF_6$ generates an asymmetrically-bridged dication $[(PPP)Co]_2[PF_6]_2$ (**3**) in which the oxidation has occurred in a delocalized fashion throughout the Co_2P_2 core. In contrast, $[(PPP)Co]_2^+$ (**5**), which can be generated either by one-electron oxidation of **2** with $FcPF_6$ or comportionation of **2** and **3**, features an asymmetric geometry and localized mixed valence. Treatment of **1** with the milder reductants $CoCp_2$ and $KBEt_3H$ does not lead to formation of **2**, **3**, or **5**, but instead generates dimeric species $[(PPP)CoCl]_2$ (**6**) and $[(PPP)CoH]_2$ (**7**). Unlike **2**-**5**, where the phosphine sidearms of the tridentate [PPP] ligand span the two Co centers, complex **6** and **7** are connected solely by NHP^- ligands that bridge the two (PPP)Co fragments.

INTRODUCTION

N-heterocyclic phosphenium cations (NHP^+s) are isolobal analogues of N-heterocyclic carbenes (NHCs) that have garnered comparatively little attention in transition metal coordination chemistry and catalysis.[1] One distinguishing feature of NHP^+s is their potential to adopt different binding modes when coordinated to a transition metal. NHP^+s most commonly adopt a trigonal planar geometry at the phosphorus atom when bound to a transition metal through lone pair σ-donation into an empty metal d orbital accompanied by π-backbonding from a filled metal d orbital into a P^{NHP}-centered π* orbital. These two interactions combine synergistically to lead to metal-phosphorus multiple bond character, akin to transition metal carbonyl complexes. In contrast, there are a few examples of NHP^+s that bind to metals exclusively through metal-to-phosphorus Z-type σ donation, resulting in a pyramidal geometry about the central phosphorus atom.[2] Alternatively, a pyramidal geometry about the phosphorus center may indicate two-electron reduction of the NHP^+ ligand to an anionic NHP^- phosphido moiety, leading to a more covalent $M\text{-}P^{NHP}$ bond. The two binding modes of $NHP^{+/-}$s and ambiguity in metal formal oxidation states that ensues draw to mind an interesting analogy to nitrosyl ligands ($NO^{+/0/-}$) ligands in their coordination chemistry, allowing $NHP^{+/-}$s to be considered as tunable versions of $NO^{+/0/-}$.[1f, 3]

To systematically explore $NHP^{+/-}$ ligands and their potential redox non-innocent behavior, our group has successfully incorporated a $NHP^{+/-}$ unit into the central position of a chelating diphosphine pincer ligand framework ($PPP^{+/-}$).[4] Coordination of the PPP^+ ligand to electron rich metals ($M = Co^{-I}$, Pt^0, Pd^0, Ni^0) has resulted in a series of monomeric complexes featuring a pyramidal geometry about the central phosphorus atom (Figure 1, **A** and **B**).[5] Both structural and computational investigations have revealed that the geometry is indicative of a stereochemically active lone pair on a negatively charged phosphido center and relatively covalent metal-phosphorus bonding. In these cases, reduction of the NHP^+ precursor to an NHP^- phosphido ligand is the result of formal two-electron oxidation of the d^{10} metal precursors. The interconversion between the NHP^+ and NHP^- configuration has been specifically attributed to the rigidity and electronic properties of the tridentate ligand framework. Delocalization of the lone pairs on the nitrogen atoms of the heterocycle into the π system of the coplanar aryl side arms has been shown to destabilize the singlet NHP^+ ground state with respect to the triplet form, promoting two-electron reduction. In the presence of just one chelating phosphine sidearm or in complexes analogous to **A** and **B** derived from NHP^+s without appended donor atoms,[3a, 6] a planar NHP^+ geometry is observed, confirming the hypothesis that pyramidalization of the phosphorus

atom is directly related to the rigid pincer ligand framework.

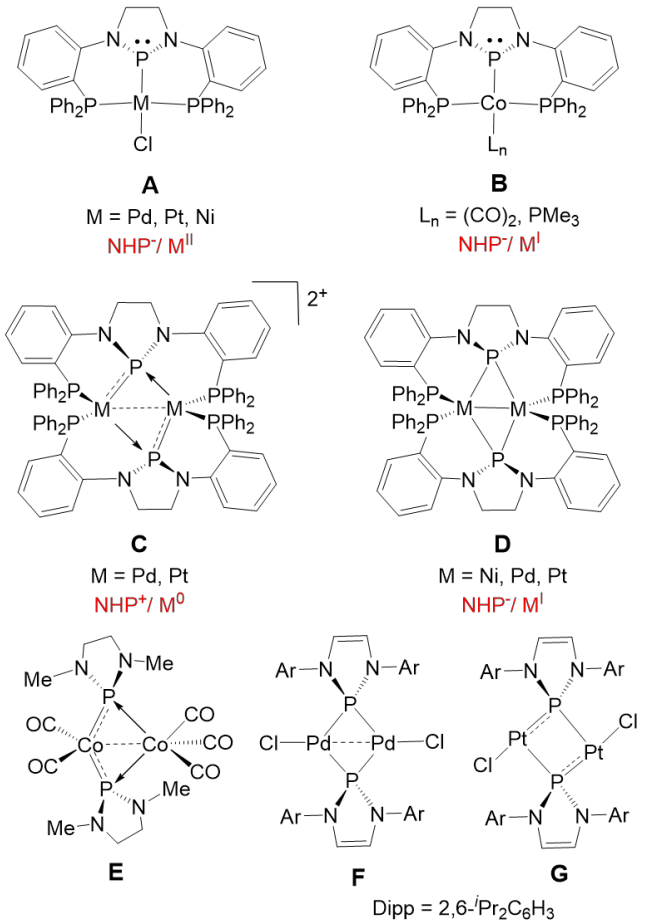

Figure 1. Selected examples of monometallic and bimetallic N-heterocyclic phosphenium (NHP^+) and phosphido (NHP^-) transition metal complexes reported by the Thomas (**A-D**),[3b, 5, 7] Hutchins (**E**),[8] and Gudat (**F**, **G**)[9] groups.

In addition to the aforementioned terminal binding modes, $NHP^{+/-}$s have been shown to bridge between two metals in multimetallic complexes. A general trend is that $NHP^{+/-}$ ligands that bridge asymmetrically are better described as NHP^+ phosphenium cations, while NHP^- ligands bridge in a symmetric fashion similar to more traditional R_2P^- phosphide ligands.[3b, 5b, 6b, 7-9] For example, our group previously reported the Group 10 $[(\mu\text{-PPP})M]_2$ (M = Ni, Pd, Pt) complexes (Figure 1, **D**) in which the four M-P^{NHP} bonds of the M_2P_2 core are nearly equivalent and the electronic structure is best described using a M^I/NHP^- formalism.[5b, 7] On the other hand, the M_2P_2 core of the dicationic $[(\mu\text{-PPP})M]_2[PF_6]_2$ (M = Pd, Pt) complexes (Figure 1, **C**) feature one short and one long M-P^{NHP} bond.[3b] The latter structural motif is also prevalent in analogous complexes comprised of monodentate NHP^+ ligands (Figure 1, **E**, **F**),[8-9] leading to a M^0/NHP^+ assignment for asymmetrically bridged complexes such as **C**. The dimeric nickel complexes have shown rich redox behavior.[5b] $[(\mu\text{-PPP})Ni]_2$ shows two well-separated oxidative waves by cyclic voltammetry (CV), and the complete $[(\mu\text{-PPP})Ni]_2^{0/+/2+}$ series is chemically accessible. The mixed valent species was identified spectroscopically, however, it was not structurally characterized and the differences in its bonding with respect to the Ni_2P_2 core were inferred through DFT calculations.[5b] Substantial structural changes to the Ni_2P_2 core were observed upon sequential oxidation in the $[(\mu\text{-PPP})Ni]_2^{0/+/2+}$ series, strongly suggesting that redox changes were shared between both the metal and the bridging phosphorus ligand (Figure 2). The redox-non-innocence of NHP^+ was recently corroborated by Gudat and coworkers, who demonstrated that one-electron reduction of (uN-HP^{Dipp})$Fe(CO)_2(NO)$ was predominantly phosphenium-centered (where $u$$NHP^{Dipp}$ is an NHP^+ ligand with 2,6-diisopropylphenyl substituents on each N atom of the unsaturated heterocylclic ring).[3d] Metal-ligand cooperative redox processes have also been reported recently by Lee and coworkers using a related bis(phosphine)phosphido pincer ligand scaffold,[10] and Peters and coworkers reported a series of dimeric bis(phosphine)phosphido and bis(phosphine)amido dicopper complexes in which redox processes were shown to involve substantial contributions from the central anionic donor.[11]

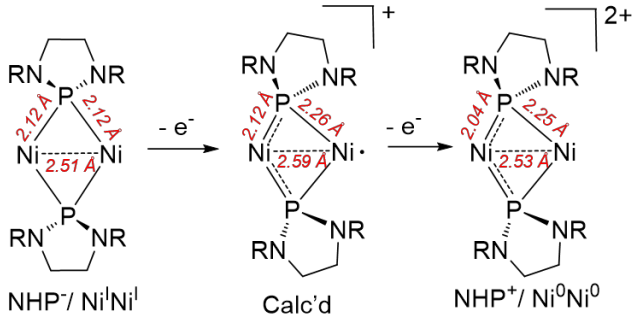

Figure 2. Structural changes to the Ni_2P_2 core upon sequential oxidation events in the $[(\mu\text{-PPP})Ni]_2^{0/+/2+}$ redox series.[5b]

Herein, we turn our attention to dimeric $NHP^{+/-}$-bridged species of cobalt to explore the generality of the geometric and electronic structural changes that occur to NHP-M scaffolds as a result of redox events. In recent studies, we have reported the monometallic complex (PPP)Co-PMe_3 (Figure 1, **B**) and successful E-H bond activation across its Co-P bond (E = H, O, S).[5a, 12] Complex **B** has not proven amenable to straightforward subsequent redox reactions.[13] Therefore, we now turn our attention to dimeric cobalt complexes of the $PPP^{+/-}$ ligand to explore the structural changes that occur with multielectron redox changes and the metal- vs. ligand-centered nature of redox processes.

RESULTS AND DISCUSSION

Synthesis and Spectroscopic Characterization of 2-7. The reduction of monometallic (PPP)M-Cl complexes (M = Pt, Pd, Ni) with 1% Na/Hg amalgam was previously shown to generate NHP-bridged homobimetallic complexes $[(\mu\text{-PPP})M]_2$ (M = Pt, Pd, Ni).[5b, 7] Using

a similar approach, the chlorophosphine-bound Co^{II} precursor $(PP^{Cl}P)CoCl_2$ (**1**)[5a] was treated with excess Mg^0 turnings in THF for 16 h to generate the Co^I/Co^I symmetric dimer complex $[(\mu\text{-PPP})Co]_2$ (**2**, Scheme 1) in 77% yield. The $^{31}P\{^1H\}$ NMR spectrum of **2** features a downfield-shifted broad singlet at 261.2 ppm and a upfield signal at 47.1 ppm in a 1:2 integral ratio, corresponding to the central halide-free NHP-derived phosphorus center and two equivalent triarylphosphine sidearms, respectively.

Scheme 1.

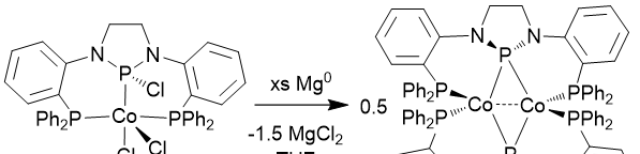

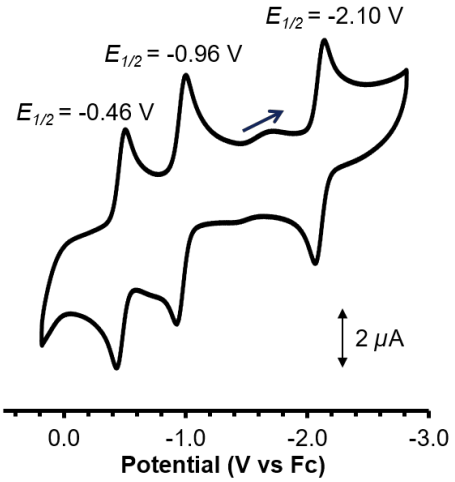

Figure 3. Cyclic voltammogram of **2** (0.3 M [^{t}Bu$_4$N][PF_6] in THF, scan rate = 100 mV s^{-1}).

To probe the redox activity of complex **2**, cyclic voltammetry measurements were performed. The cyclic voltammogram (CV) of **2** reveals three one-electron processes: two well-separated reversible oxidations at -0.96 V and -0.46 V and a reduction at -2.10 V (vs. the ferrocene/ferrocenium couple, Fc/Fc^+, Figure 3). Attempts at isolating a one-electron reduction product by chemically reducing **2** were unsuccessful. The 500 mV separation of the two reversible oxidations of **2** leads to an estimated comproportionation constant (K_c) of 3×10^8. The CV of the analogous Ni^I/Ni^I dimer, $[(\mu\text{-PPP})Ni]_2$, also features two reversible oxidative waves, but at more negative potentials (-1.05 V and -0.70 V).[5b] Unlike **2**, the CV of the $[(\mu\text{-PPP})Ni]_2$ dimer does not contain any reductive features within the solvent-accessible window.[5b] Both of these observations are consistent with the less electron-rich nature of **2** compared to $[(\mu\text{-PPP})Ni]_2$ as a result of the two additional *d* electrons in the dinickel complex. In the nickel case, the smaller peak separation of 340 mV results in a smaller K_c of 5.6×10^5, indicative of a less thermodynamically stable mixed valence species. Both oxidations of the $[(\mu\text{-PPP})Ni]_2$ dimer could be successfully accessed using chemical oxidants, however, the one-electron oxidized mixed valence species could not be crystallographically characterized due to disproportion and co-crystallization of the desired monocationic species with the neutral precursor.[5b] The larger peak separation and K_c observed in the CV of dicobalt complex **2** suggests that isolation of a complete series of $[(\mu\text{-PPP})Co]_2^{0/+/2+}$ complexes is possible.

Scheme 2.

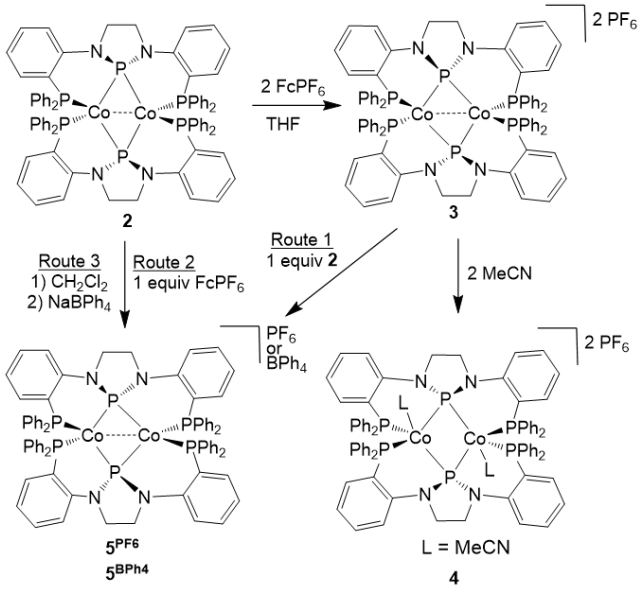

Inspired by the reversible oxidative events observed in the CV of **2**, we next explored the chemical oxidation of **2**. The addition of two equivalents of $FcPF_6$ to **2** cleanly generated the two-electron oxidized complex $[(\mu\text{-PPP})Co]_2[PF_6]_2$ (**3**, Scheme 2) in 90% isolated yield. The $^{31}P\{^1H\}$ spectrum of **3** contains three new resonances in a 1:2:1 integral ratio, including two broad multiplets at 225.9 ppm and 29.6 ppm corresponding to the two central bridging phosphorus atoms and four equivalent phosphine side-arms, respectively, and a septet at -144.4 ppm for the two PF_6^- anions. In the presence of acetonitrile, complex **3** undergoes a color change from dark red to purple, generating the acetonitrile adduct $[(\mu\text{-PPP})Co(NCMe)]_2[PF_6]_2$ (**4**, Scheme 2) in 85% yield. The $^{31}P\{^1H\}$ NMR spectrum of **4** is reflective of a considerably less symmetric structure in solution, and contains four signals of equal integration, corresponding to the P^{NHP} moiety (215.5 ppm), inequivalent phosphine side-arms (43.1 ppm and 20.0 ppm), and the PF_6^- counteranions (-143.4 ppm).

A monocationic mixed valence species was subsequently targeted to complete the redox series. As predicted based on the aforementioned large K_c estimated from the CV of **2**, comproportionation of a 1:1 mixture

of complexes **2** and **3** affords the monocationic complex [(μ-PPP)Co]$_2$[PF$_6$] (**5^{PF6}**, Scheme 2, Route 1) in 68% yield. The mixed valence cation can also be synthesized via two alternate routes. Oxidation of **2** with one equivalent of FcPF$_6$ affords **5^{PF6}** (Scheme 2, Route 2) in 78% yield. Alternatively, stirring **2** in dichloromethane for 16 h at room temperature initially generates **5^{Cl}** and subsequent anion exchange with NaBPh$_4$ or NaPF$_6$ affords **5^{BPh4}** or **5^{PF6}** (Scheme 2, Route 3) in 89% or 91% yield, respectively. The ^{1}H NMR spectra of **5^{x}** do not vary as a function of counterion and contain broad resonances with chemical shifts ranging from -19 to 0 ppm, indicative of a paramagnetic compound. Complex **5^{x}** is also ^{31}P{^{1}H} NMR silent except for the resonance corresponding to the PF$_6^-$ counterion in the case of **5^{PF6}**. Evans' method provides a solution-state magnetic moment measurement of μ_{eff} = 1.68 μ_B, which is consistent with an S = ½ spin state.[14] The EPR spectrum of **5^{Cl}** in frozen THF solution provides further insight into the electronic structure of the monocation (Figure 4). The EPR signal for **5^{Cl}** is nearly axial signal with g values of 2.27, 2.05, and 2.02, consistent with a cobalt-centered radical. Although no distinct hyperfine features can be resolved, the spectrum can be satisfactorily simulated by invoking relatively small hyperfine coupling to a single ^{59}Co (I = 7/2) center (A = 67, 40, 0 MHz); however, electron delocalization onto the second ^{59}Co center cannot be ruled out owing the broad nature of the signal.[15]

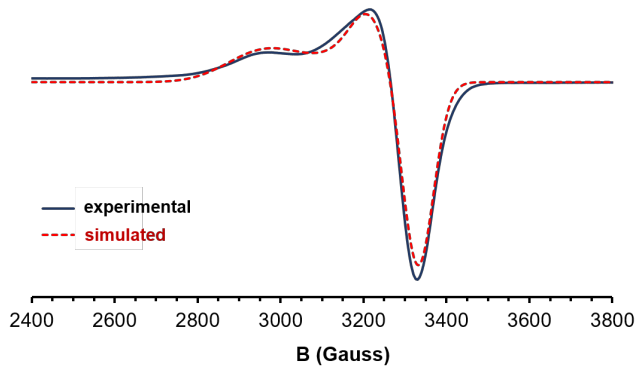

Figure 4. Experimental (black) and simulated (red, dotted) X-band (9.38 GHz) EPR spectrum of **5^{Cl}** in frozen THF at 4 K (modulation amplitude = 5 G, power = 20 mW).

The monocationic complex **5^{X}** could not be synthesized directly from **1** via addition of milder reducing agents, as a different dimeric species was isolated under these conditions. The addition of a milder reductant such as CoCp$_2$ to complex **1** results in a drastic color change from orange to dark green and the generation of a new two-electron reduced diamagnetic species [(PPP)CoCl]$_2$ (**6**) in 75% yield. Complex **6** is a dimeric species in which two monomeric (PPP)CoCl units are bridged through the P^{NHP} moieties. In contrast to dimers **2**-**5**, the triarylphosphine sidearms of the ligand in **6** are both bound to the same metal rather than spanning two cobalt centers (*vide infra*). The ^{31}P{^{1}H} NMR spectrum of **6** contains three resonances in a 1:1:1 ratio, including a downfield doublet at 218.7 ppm, corresponding to the P^{NHP} atoms, and a singlet at 40.6 ppm and doublet at 16.7 ppm corresponding to the two sets of inequivalent triarylphosphine sidearms on each half of the dimer. In the ^{1}H NMR spectrum of **6** there are four resonances between 2.5 and 4.0 ppm corresponding to the protons of the NHP backbone, which is consistent with the asymmetry observed in both the ^{31}P{^{1}H} NMR spectrum and the solid state structure (*vide infra*). Crystallographic and DFT analysis supports the assignment of complex **6** as an NHP$^-$ phosphido ligand bound to Co^{II} (*vide infra*); however, the diamagnetism of complex **6** can only be achieved by antiferromagnetic coupling of the two Co(PPP) units regardless of how you assign the oxidation state of Co or the charge on the NHP$^{+/-}$ ligand. Complex **6** can be further reduced to complex **2** upon the addition of a strong reductant, Mg^0.

Scheme 3.

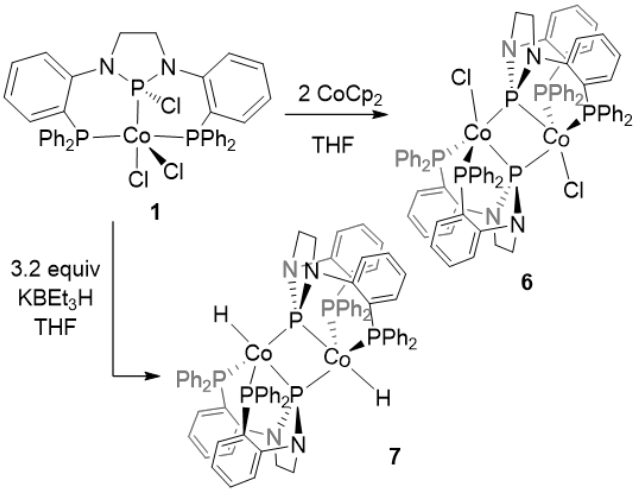

Reduction of **1** with a hydride-containing reductant instead generates a hydride derivative of **6**. Addition of 3.2 equivalents of KBEt$_3$H to **1** in THF resulted in transformation of the initial orange suspension into a homogenous dark red solution containing the new diamagnetic species [(PPP)CoH]$_2$ (**7**), which adopts a bridging coordination motif similarly to **6** and can be isolated in 90% yield. The ^{31}P{^{1}H} NMR spectrum of **7** contains two resonances at 289.6 ppm and 45.6 ppm that integrate in a 1:2 ratio corresponding to the P^{NHP} atoms and the equivalent triarylphosphine sidearms, respectively. The ^{1}H NMR spectrum of **7** is also consistent with a C_{2v}-symmetric structure, as only two resonances are observed for the protons of the NHP backbone. In addition, a broad ^{1}H NMR signal at -8.3 ppm diagnostic of a metal hydride is observed. The equivalent phosphine sidearms and the presence of only two backbone proton resonances indicates that **7** adopts a more symmetric geometry in solution than its chloride congener **6**, which has three ^{31}P{^{1}H} NMR resonances and four ^{1}H NMR signals for the NHP backbone protons. Similar to complex **6**, the diamagnetism of **7** is achieved through the antiferromagnetic

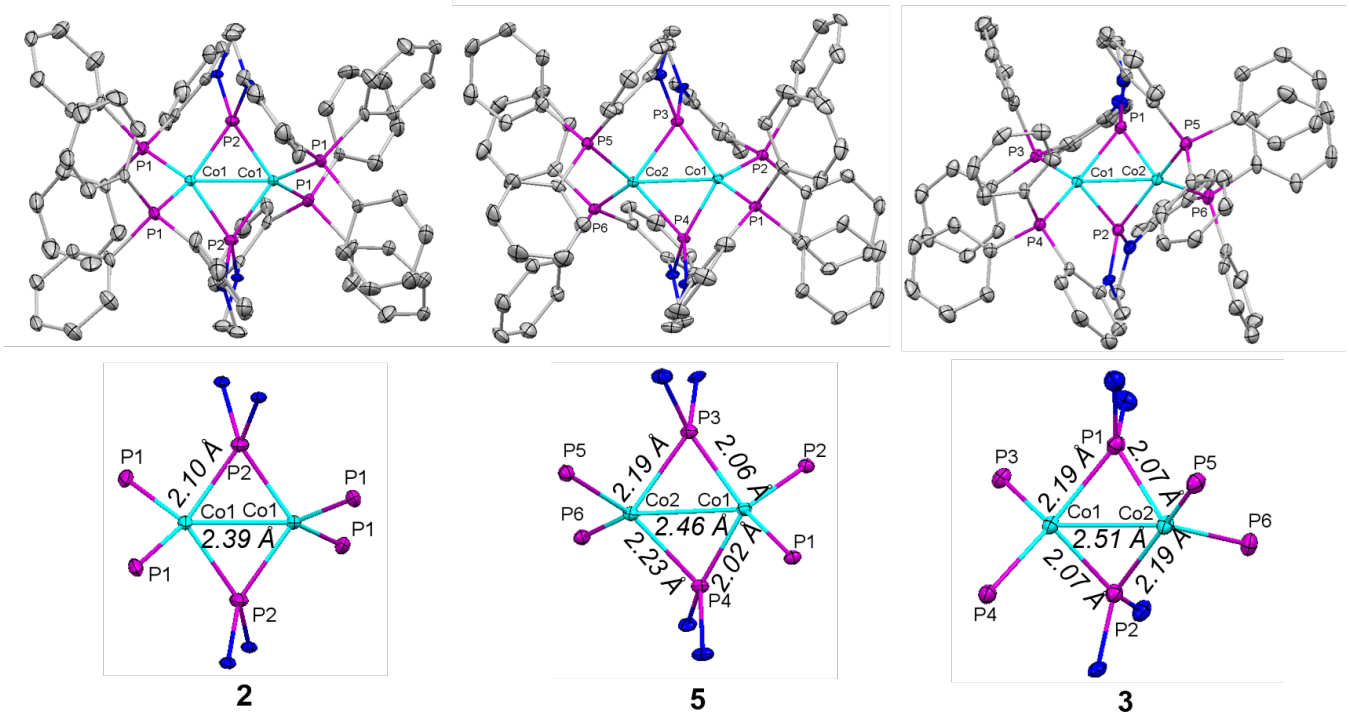

Figure 5. Top: Displacement ellipsoid (50%) representation of **2**, **3**, and $\mathbf{5}^{\mathbf{BPh4}}$. All hydrogen atoms, counterions, and solvate molecules have been omitted for clarity. Bottom: Co_2P_2 cores of **2**, **5**, and **3** with relevant interatomic distances labelled.

coupling of two (PPP)CoH units (*vide infra*). Complex **7** is unable to be further reduced to complex **2**, however complex **7** decomposes to complex **2** if left in solution for multiple days.

Structural Characterization of 2-7. The solid-state structure of **2** determined by single crystal X-ray diffraction confirms its formulation as a highly symmetric dimer that is isostructural to the previously reported $[(PPP)Pt]_2$ and $[(PPP)Ni]_2$ complexes (Figure 5).[5b, 7] The Co_2P_2 diamond core of **2** contains four crystallographically equivalent P^{NHP}-Co bond distances of 2.0957(13) Å and a Co-Co distance of 2.3865(15) Å. The P^{NHP}-Co bond distances are shorter than in the previously reported monomeric complex $(PPP)Co(CO)_2$ (2.2386(6) Å).[5c] The Co-P^{NHP} and Co-Co bond distances are both at the shorter extreme compared to previously reported symmetric Co_2P_2 bridging PR_2^- complexes, which range from 2.1-2.3 Å and 2.3-3.5 Å, respectively.[16] The short Co-Co distance in **2** is consistent with a Co-Co single bond.[17] The sum of the internal angles of the Co_2P_2 core is 360°, and the rigorously planar Co_2P_2 core is similar to that of Mindiola's $(PNP)_2Co_2$ (PNP = $[N\{2\text{-}P^iPr_2\text{-}4\text{-}MeC_6H_3\}_2]^-$) complex.[18] In contrast, Arnold's analogous $\{N(CH_2CH_2P^iPr_2)\}_2Co_2$ complex, in which the tridentate ligand has aliphatic rather than aromatic linkers between the donor atoms, has a butterfly Co_2N_2 core (sum of internal angles = 333°).[19] The symmetric nature of **2** and the structural similarities between **2** and both related Co^I/Co^I dimers[18-19] and analogous $(\mu\text{-PPP})_2M^I_2$ dimers (M = Ni, Pd, Pt),[5b, 7] suggest that complex **2** is best described as a dicobalt(I) dimer bridged by two NHP^- phosphido ligands.

Upon one-electron oxidation, single crystal X-ray structure determination reveals that the Co_2P_2 central diamond core of mixed valence monocation $\mathbf{5}^{\mathbf{BPh4}}$ becomes asymmetric (Figure 5). Both of the bridging NHP ligands feature much shorter Co-P^{NHP} bond distances to one of the two Co centers (2.0593(10) Å, 2.0218(11) Å), with elongated bond distances to the second Co atom (2.1887(11) Å and 2.2258(10) Å). The Co_2P_2 core has little distortion from planarity, but the asymmetry in Co-P^{NHP} distances is accompanied by a change in the planarity/pyramidalization of the NHP binding mode. The angle between the N-P-N planes and the shorter Co-P bond vectors are 157° while the angle between the N-P-N plane and the elongated Co-P^{NHP} bonds are 134°. Both the more planar binding mode and the shorter Co-P^{NHP} distances are suggestive of a substantial reorganization of the electronic structure of the Co_2P_2 core compared to neutral precursor **2** and a localized mixed valence state. However, it is not possible to determine whether the electronic structure of $\mathbf{5}^{\mathbf{BPh4}}$ is most accurately described as $Co^{II}/Co^I/NHP^-$ or $Co^0/Co^{-I}/NHP^+$. The Co-Co distance in $\mathbf{5}^{\mathbf{BPh4}}$ (2.4652(7) Å) is elongated compared to **2**, but is still indicative of some degree of metal-metal bonding.[20]

The solid-state structure of complex **3** determined by single crystal X-ray diffraction also revealed a distortion of the Co_2P_2 core upon two-electron oxidation

(Figure 5). The Co_2P_2 core of **3** is asymmetric, with each Co center binding to the two bridging P^{NHP} atoms through one short (2.0669(16) Å, 2.0711(16) Å) and one long (2.1879(17) Å, 2.1916(17) Å) Co-P^{NHP} bond per Co atom in an alternating arrangement similar to the Pd and Pt analogues.[3b] The Co_2P_2 core in **3** is also distorted out-of-plane into a butterfly shape and the sum of internal angles of the Co_2P_2 core is 339°. The Co-Co distance of 2.5118(11) Å is elongated compared to both **2** and **5**, but remains short enough to indicate bonding interactions between the two Co atoms.[21] In the related $[(\mu\text{-PPP})M]_2[PF_6]_2$ (M = Pd, Pt) complexes, the difference in M-P^{NHP} distances was more pronounced (0.3 Å).[3b] Furthermore, the NHP ligands were tilted to adopt a more planar geometry towards the metal with the shorter M-P distance as measured by very different angles between the N-P-N plane and the short and long M-P bond vectors (164.5° and 122.5°, respectively). In contrast, the Co-P^{NHP} distances in **3** only differ by 0.1 Å and there is a negligible difference in the angles between the N-P-N plane and the short and long Co-P bond vectors (145° and 144°). Thus, the assignment of cobalt oxidation state and $NHP^{+/-}$ phosphenium/phosphido is far more ambiguous than in the Group 10 analogues and necessitates further spectroscopic studies.

The solid-state structure of **4** determined by single crystal X-ray diffraction revealed a dicationic bimetallic complex similar to **3** but with one acetonitrile molecule coordinated to each metal center (Figure S32). The Co-Co distance is elongated to 2.7752(16) Å in **4**, indicating disruption of any significant metal-metal bonding upon coordination of an ancillary ligand. Although the Co_2P_2 core of **4** also adopts a butterfly geometry (sum of internal angles = 329°), unlike **3**, **4** contains four similar Co-P bond distances around 2.14 Å. The asymmetry of **4** observed in solution by NMR spectroscopy is consistent with the solid-state structure, which features a dihedral angle (MeCN-Co-Co-NCMe) of -114° that renders the two phosphine sidearms of each PPP ligand inequivalent.

The solid-state structure of **6** determined by single crystal X-Ray diffraction confirmed a dimeric structure, with the two cobalt centers bridged through the central NHP phosphorus atom (Figure 6). Unlike **2**, the aryl side arms of each ligand in **6** are bound to the same metal atom rather than spanning the two Co centers. The inequivalence of the phosphine side arms and NHP backbone protons observed spectroscopically is consistent with the solid-state structure, which lacks a mirror plane and features a Cl1-Co1-Co2-Cl2 dihedral angle of -123.2°. Monomeric 16-electron analogues of complex **6** have been isolated for Ni, Pd, and Pt ((PPP)MX, M = Ni, X = Cl; M = Pd, Pt, X = Cl, Br, I).[5b, 7] The dimerization in the case of cobalt is likely the result of the more electron poor cobalt center and the ability to form a closed shell configuration upon dimerization. The Co-P^{NHP} distances within each internal (PPP)Co unit in **6** (2.0737(11)

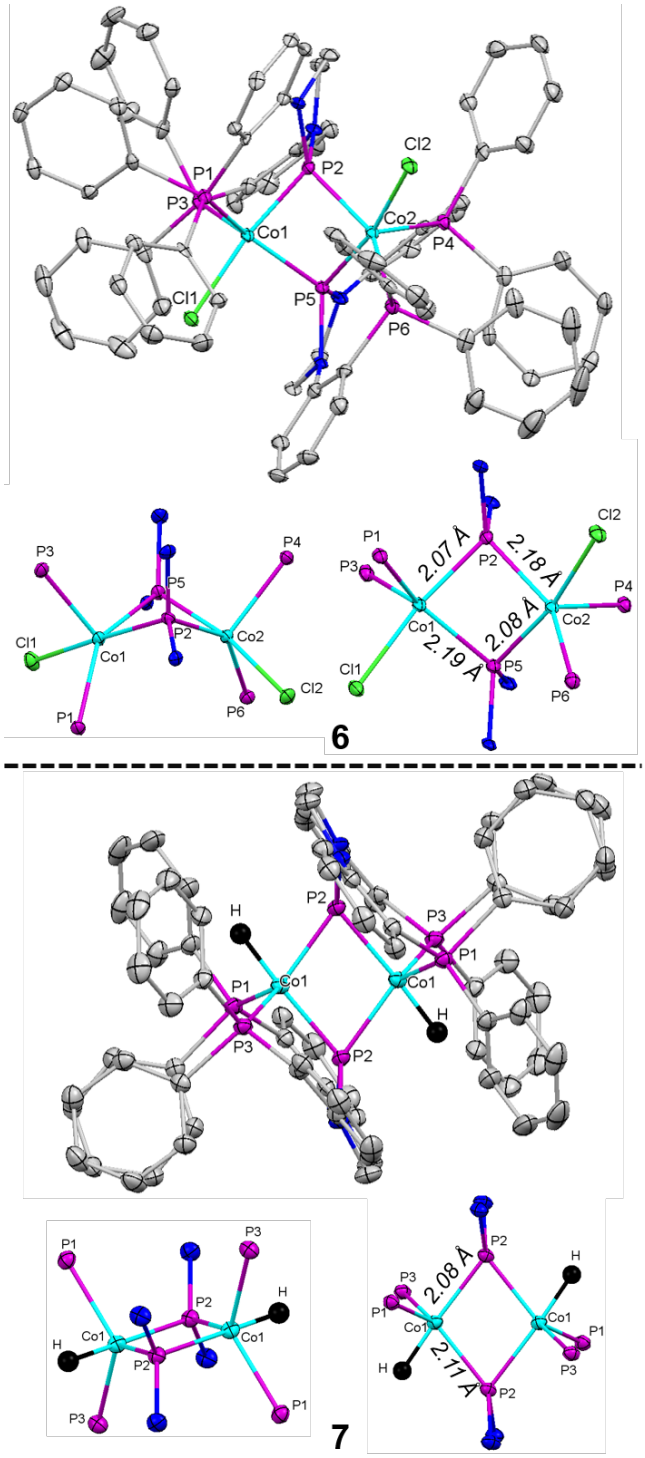

Figure 6. Displacement ellipsoid (50%) representation of **6** (top) and **7** (bottom) including truncated Co_2P_2 cores with relevant interatomic distances. For clarity, only one of two independent molecules in the asymmetric unit of **7** is shown, and all solvate molecules and hydrogen atoms except for the hydride ligands have been omitted.

Å and 2.0781(11) Å) are comparable to both the Co-P distances in **2** and the shorter Co-P distances in asymmetric complexes **3** and $\mathbf{5}^{BPh4}$. Each NHP phosphorus atom then bridges to the second (PPP)Co unit through longer Co-P^{NHP} bonds (2.1902(11) Å and 2.1825(11) Å) that are

comparable to the longer Co-P distances in **3** and **5**^{BPh4}. The NHP ligands adopt pyramidal geometries with respect to the Co centers within each (PPP)Co monomeric unit, and can be described using either NHP^{-}/Co^{II} or NHP^{+}/Co^{0} formalisms. In either case, however, antiferromagnetic coupling of the two fragments must be invoked to achieve a diamagnetic ground state. In the case of **6**, the Co-Co distance is too long to be associated with a metal-metal bond 2.8727(7) Å.

Single crystal X-ray diffraction confirmed the identity of **7** as a phosphorus-bridged dimer analogous to **6** (Figure 6). Unlike **6**, complex **7** is symmetric in the solid state: The H-Co-Co-H dihedral angle in **7** is 0°, indicating a planar Co_2P_2 core and a mirror plane containing the P, Co, and H atoms, which is consistent with the solution NMR data (*vide supra*). The Co-P^{NHP} distances within each monomeric (PPP)Co fragment in **7** are comparable to those in **6**, however, the Co-P^{NHP} distances through which the two monomers are bridged are 0.08 Å shorter than in **6**. The Co-Co distance is also significantly shorter in **6** (2.5747(5) Å) than in **7**, but this may be due to geometric constraints associated with the different core geometry rather differences in Co-Co bonding interactions.. As with complex **6**, both NHP^{-}/Co^{II} and NHP^{+}/Co^{0} descriptions are possible for complex **7**, and the two monomeric units must be antiferromagnetically coupled to yield a diamagnetic complex (*vide infra*).

Computational Investigations. To provide further insight into the nature of the Co-P^{NHP} bonds in **2-7** and the structural differences associated with the Co_2P_2 core upon redox changes, computational studies were carried out using density functional theory (DFT). Geometry optimizations were performed starting from crystallographically derived Cartesian coordinates, and the computed bond metrics were in agreement with those determined by X-Ray crystallography (Tables S4-S5).

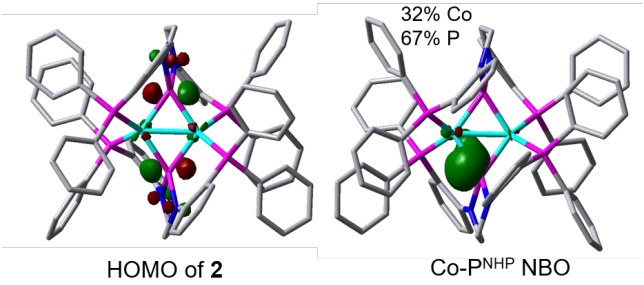

Figure 7. Pictorial representations of the calculated HOMO (left) and one representative Co-P^{NHP} natural bond orbital of **2** (right).

Examination of the calculated frontier molecular orbitals of the symmetric dimer **2** sheds light on the structural rearrangements that occur upon oxidation of this complex. The highest occupied molecular orbital (HOMO) of **2** is centered almost entirely on the phosphorus p orbitals of the bridging P^{NHP} functionalities, with very little contribution from the cobalt d orbitals (Figure 7, left). This observation is consistent with a reduced Co^{I}/Co^{I} phosphido description and the fact that one- or two-electron oxidation of **2** involves substantial rearrangement of the geometric and electronic structure of the Co_2P_2 core. Natural bond orbital (NBO) analysis of **2** reveals four similar Co-P^{NHP} NBOs comprised of roughly 32% Co and 67% phosphorus character (Figure 7, right). Inspection of the frontier orbital region of **2** also reveals several orbitals with substantial orbital overlap between the two Co centers (Figure S36); however, the net result of population of both bonding and anti-bonding orbitals is, at most, a metal-metal single bond (Co-Co Mayer bond order = 0.89; see Table S7).

Table 1. Computed natural charges on the Co and P^{NHP} atoms in **2**, **3**, **5**, **5'**, **6**^{monomer} and **7**^{monomer}.

Complex	Natural Charges	
	Co	P
$[(\mu\text{-PPP})Co]_2$ (**2**)	-1.42 -1.42	1.44 1.44
$[(\mu\text{-PPP})Co]_2^{+}$ (**5**)	-1.72 -0.42	1.52 1.54
$[(\mu\text{-PPP})Co]_2^{+}$ (**5'**)	-1.07 -1.07	1.60 1.60
$[(\mu\text{-PPP})Co]_2^{2+}$ (**3**)	-1.06 -1.06	1.68 1.68
(PPP)CoCl (**6**^{monomer})	-0.59	1.23
(PPP)CoH (**7**^{monomer})	-0.67	0.935

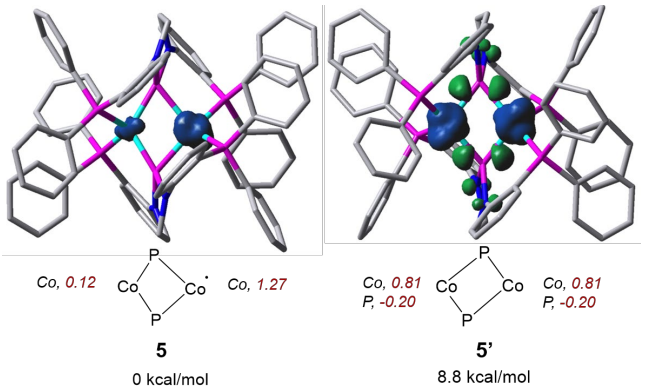

Figure 8. Unpaired spin density surfaces of **5** and **5'**. Computed Mulliken spin density values on the Co and P atoms are indicated in red.

Upon oxidation to complex **5**, the bonding in the asymmetric Co_2P_2 core changes significantly as reflected by the Co-P bond distances. The unpaired spin density of **5** is located predominately on the Co center with elongated Co-P^{NHP} bonds, suggesting a localized mixed valence state (Figure 8, left). In addition, the computed natural charges on the two Co atoms are significantly different (-1.72 and -0.42) and indicate that one-electron oxidation occurred at the Co center with longer Co-P^{NHP} distances (Table 1). The computed natural charges on the

P^{NHP} atoms in **5** also increase upon oxidation from neutral complex 2, in line with removal of an electron from an orbital with substantial phosphorus character. The localization of the unpaired spin density of **5** is similar to that predicted previously for $[(\mu\text{-PPP})Ni]_2^+$.[5b] The Co-Co Mayer bond order calculated for **5** (0.61) indicates diminished metal-metal bonding compared to **2**, consistent with the longer interatomic distance (*vide supra*).

A second energetic minimum 8.8 kcal/mol higher in energy than **5** was found when starting the geometry optimization from a symmetric core geometry (i.e. starting with the X-ray derived coordinates of **2**). In this case, the geometry optimization proceeds to **5'**, which has an asymmetric core structure more similar to that of complex **3**, with each cobalt center having one short and one long bond to a bridging P^{NHP} atom. In contrast to **5**, **5'** exhibits delocalized mixed valence with unpaired spin density delocalized throughout the Co_2P_2 core. In agreement with the delocalized description of the one-electron oxidation, the natural charges on both the Co and P atoms increase by 0.41 and 0.16, respectively, upon oxidation from **2** to **5'**. Based on these computational results, it seems reasonable that oxidation initially occurs via removal of an electron from the phosphorus-based HOMO of **2**, followed by geometric relaxation to **5'**. The delocalized unpaired spin density of **5'** is consistent with the large (500 mV) experimental difference between the first and second oxidation potentials of **2**. Complexes **5'** and **5**, which has a more localized asymmetric geometry, may interconvert readily in solution and it is possible that the asymmetric geometry observed in the solid state structure of **5** is an artifact of crystal-packing effects. .

Geometry optimization of **3** leads to an asymmetric Co_2P_2 core in which each cobalt center has one short P^{NHP} bond and one long P^{NHP} bond, consistent with the solid state structure shown in Figure 5. The Co-Co Mayer bond order calculated for **3** (0.71) indicates that metal-metal bonding interactions remain upon two-electron oxidation. Despite the significant differences in Co-P^{NHP} distances in the Co_2P_2 core, NBO analysis finds all four Co-P^{NHP} orbitals to have similar atomic compositions from Co (35%) and P (65%**)** character (Figure S37). The natural charges on the Co centers in **3** are 0.36 more positive than the Co centers in **2** while the P^{NHP} atoms are 0.23 more positive than in **2**, suggesting that both Co and P participate in the two-electron oxidation from **2** to **3** (Table 1).

Rather than computing the dimers **6** and **7**, we found it more constructive to computationally explore the differences in the electronic structure and bonding of their monomeric components (PPP)CoCl (**6**$^{\textbf{monomer}}$) and (PPP)CoH (**7**$^{\textbf{monomer}}$) to better understand the origin of the geometric differences between **6** and **7**. In both cases, an $S = 1/2$ ground state was predicted for the monomeric species, with the quartet state calculated to be significantly higher in energy (Table S8). The DFT-optimized structures of **6**$^{\textbf{monomer}}$ and **7**$^{\textbf{monomer}}$ feature significantly different geometries about the Co centers, with **6**$^{\textbf{monomer}}$ adopting a distorted tetrahedral geometry ($\tau_4 = 0.77$) and **7**$^{\textbf{monomer}}$ adopting a geometry much closer to square planar ($\tau_4 = 0.24$).[22] The different geometric preferences of the monomeric fragments are likely the underlying cause of the different geometric arrangements observed upon dimerization to complexes **6** and **7**. Furthermore, the geometric differences between **6**$^{\textbf{monomer}}$ and **7**$^{\textbf{monomer}}$ are accompanied by large differences in electronic structure that can best be visualized by examining the unpaired spin density surfaces of the complexes (Figure 9). The unpaired spin in hydride complex **7**$^{\textbf{monomer}}$ resides almost exclusively on the Co atom in a d_{z2}-like orbital, as would be expected for a low spin square planar Co^{II} complex. In contrast, **6**$^{\textbf{monomer}}$ features unpaired spin density distributed between both the Co and P^{NHP} atoms, with an α spin of 1.30 on Co and β spin of -0.28 on the P^{NHP} atom. This may suggest that there may also be substantial differences in the way that the two Co^{II} centers in **6** and **7** are antiferromagnetically coupled, with substantially more ligand contributions to magnetic exchange in chloride complex **6**.

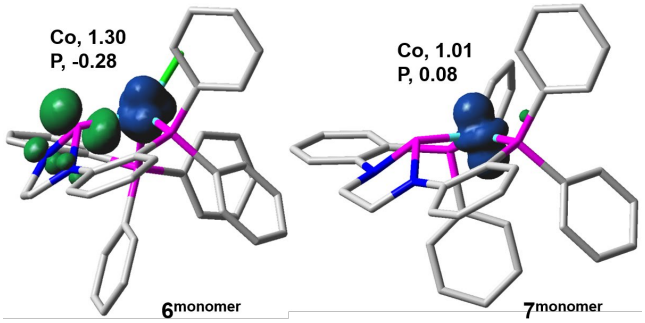

Figure 9. Unpaired spin density surfaces of **6**$^{\textbf{monomer}}$ and **7**$^{\textbf{monomer}}$ with computed Mulliken spin density values on the Co and P atoms indicated.

Conclusions

In summary, by varying the choice of reducing agent, a series of dimeric species with different electronic structures and NHP bridging modes can be synthesized from the Co^{II} dichloride complex **1**. Reduction of **1** with a strong reductant (Mg^0) affords a Co^ICo^I bis(phosphido)-bridged dimer **2** that can be oxidized in two sequential steps to afford a complete $[(PPP)Co]_2^{0/+/2+}$ redox series. All three $[(PPP)Co]_2^{0/+/2+}$ compounds were successfully isolated and crystallographically and spectroscopically characterized, revealing distinct changes to the geometry and bonding within the Co_2P_2 core as a function of redox events. Computational results suggest that one-electron oxidation of **2** is phosphorus ligand-centered, but that subsequent structural rearrangement leads to changes in the Co-P^{NHP} bonding patterns within the Co_2P_2 core. These structural and electronic rearrangements ultimately

afford a localized mixed valence complex **5** that is effectively the product of one-electron oxidation at a single Co site. A second one-electron oxidation affords **3**, whose geometry and electron localization are more symmetric in nature. The reduction of **1** with the milder reductants $CoCp_2$ and $KBEt_3H$ generates the dimeric species **6** and **7**, respectively. While the side arms of the PPP ligand in **2**-**5** span the two Co centers, complexes **6** and **7** are linked exclusively through the bridging NHP^- ligands. Pt^{II}, Pd^{II}, and Ni^{II} complexes similar to **6** have been synthesized previously, but remained monomeric owing to the inherent stability of the 16-electron d^8 square planar configuration. However, the assignment of metal oxidation state and determination of whether the $NHP^{+/-}$ ligand is in the phosphenium/phosphido state is far more ambiguous for **2**-**7** compared to the Group 10 analogues. Further spectroscopic studies including Co K-edge X-ray absorption near edge spectroscopy (XANES) are planned to more accurately assess the electronic structure of these compounds. Nonetheless, since both cobalt and phosphorus appear to be involved in the redox processes reported herein, the (PPP)Co framework may provide a fruitful platform for exploring catalytic applications and this will be subject of future studies.

EXPERIMENTAL SECTION

General Considerations. Unless otherwise noted, all manipulations were carried out under an inert atmosphere using a nitrogen-filled glovebox or standard Schlenk techniques. Glassware was oven-dried before use. Diethyl ether, tetrahydrofuran, toluene, dichloromethane, and benzene were degassed by sparging with ultra-high purity argon and dried via passage through columns of drying agents using a Seca solvent purification system from Pure Process Technologies. Benzene-d_6 was degassed via repeated freeze-pump-thaw cycles and dried over 3 Å molecular sieves before use. CD_2Cl_2 was dried over CaH_2 for 2 days followed by vacuum transferring to an oven-dried vessel. Dry CD_2Cl_2 was then degassed via repeated freeze pump-thaw cycles and stored over 3 Å molecular sieves. ($PP^{Cl}P$)$CoCl_2$ (**1**) was synthesized according to literature procedures.[5a] All other reagents and solvents were obtained from commercial sources and used without further purification. NMR spectra were recorded at ambient temperature unless otherwise stated on a Varian Inova 400 MHz, Varian MR 400 MHz, Bruker DPX 400 MHz, or Bruker 600 MHz Avance III HD instrument. ^1H and ^{13}C NMR chemical shifts were referenced using residual solvent resonances and are reported in ppm. $^{31}P\{^1H\}$ NMR chemical shifts (in ppm) were referenced using an external standard (85% H_3PO_4, 0 ppm). ^{19}F NMR chemical shifts are referenced using an external standard (1% trifluoroacetic acid, -76.5 ppm). ^{11}B NMR chemical shifts are referenced using an external standard (BF_3•Et_2O, 0 ppm). Evans method was used to measure solution magnetic moments.[14] Satisfactory elemental analysis data could not be obtained owing to the air and moisture sensitive nature of the compounds, therefore HRMS (ESI) was performed.

Synthesis of [(μ-PPP)Co]$_2$ (2). Complex **1** (46 mg, 0.059 mmol) was suspended in THF (8 mL). Mg turnings (12 mg, 0.49 mmol) were added to a solution the frozen solution of **1**. The resulting mixture was stirred for 18 hours at room temperature. The red solution was filtered through Celite and solvent was removed from the filtrate in vacuo. The resulting crude red/orange oil was washed with cold toluene (2 x 3 mL) and the solid was collected and dried in vacuo yielding pure **2**. Another batch of **2** was collected by removing the toluene in vacuo and washing the resulting solid with cold toluene (2 x 3 mL) and collecting the solid (31 mg, 77%). Crystals of **2** suitable for X-ray diffraction were grown via vapor diffusion of pentane into a concentrated THF solution of **2**. ^1H NMR (600 MHz, C_6D_6): δ 7.23 (br m, Ar-H, 8H), 7.06 (m, Ar-H, 10H), 7.01 (t, Ar-H, 6H), 6.97-6.90 (m overlapping signals, Ar-H, 16H), 6.71 (t, J_{H-P} = 8 Hz, Ar-H, 8H), 6.34 (t, J_{H-P} = 8 Hz, Ar-H, 4H), 5.95 (s, Ar-H, 4H), 3.88 (br m, CH_2, 4H), 3.34 (br m, CH_2, 4H). $^{31}P\{^1H\}$ NMR (242.8 MHz, C_6D_6): δ 261.2 (s, central, 2P), 47.1 (s, sidearm, 4P). $^{13}C\{^1H\}$ NMR (150.8 MHz, C_6D_6): δ 148.9 (s), 136.5 (s), 134.3 (s), 134.1-133.8 (two overlapping signals), 130.9 (s), 127.7 (overlapping with solvent peak), 127.0 (s), 119.5 (s), 117.7 (s), 48.8 (s, CH_2). UV-Vis (THF, λ(nm) (ε, $M^{-1}cm^{-1}$): 400 (1.7 x 10^4), 540 (3.4 x 10^3). HRMS (ESI): Calcd *m/z* for **2**: 1336.2221; Found: 1336.2225.

Synthesis of [(μ-PPP)Co]$_2$[PF_6]$_2$ (3): Complex **2** (43 mg, 0.032 mmol) was dissolved in THF (5 mL). $FcPF_6$ (24 mg, 0.071 mmol) was dissolved in THF (4 mL) and added to the stirring solution of **2**. The resulting solution was stirred at room temperature for 16 hours. The solution was filtered through Celite and solvent was removed from the filtrate in vacuo. The crude oil was washed with Et_2O (3 x 3 mL) and the solid was collected and dried in vacuo yielding pure **3** (47 mg, 90 %). Crystals of **3** suitable for X-ray diffraction were grown via layering Et_2O onto a concentrated CH_2Cl_2 solution of **3**. ^1H NMR (600 MHz, CD_2Cl_2): δ 7.40 (br m Ar-H, 12H), 6.97-7.05 (br m, Ar-H, 20H), 6.82 (br m, Ar-H, 12H), 6.60 (br m, Ar-H, 8H), 6.20 (br m, Ar-H, 4H), 3.37 (br m, CH_2, 4H), 3.18 (br m, CH_2, 4H). $^{31}P\{^1H\}$ NMR (242.8 MHz, CD_2Cl_2): δ 225.9 (br m, NHP, 2P), 29.6 (br m, PPh_2, 4P), -144.4 (septet, J_{P-F} = 710 Hz, PF_6, 2P). $^{13}C\{^1H\}$ NMR (150.8 MHz, CD_2Cl_2): δ 146.6 (s), 134.2 (s), 133.3-133.1 (2 overlapping signals), 132.9 (d, J_{C-P} = 10 Hz) 132.4 (s), 131.9 (s), 130.4 (d, J_{C-P} = 9 Hz), 129.7 (d, J_{C-P} = 9 Hz), 127.8 (d, J_{C-P} = 49 Hz), 127.0 (s), 125.1 (d, J_{C-P} = 44 Hz), 122.5 (s), 121.9 (d, J_{C-P} = 49 Hz), 52.7 (s, *C*H_2). ^{19}F NMR (564.5 MHz, CD_2Cl_2): δ -73.09 (d, J_{F-P} = 710 Hz, PF_6, 6F). UV-Vis (THF, λ(nm) (ε, $M^{-1}cm^{-1}$): 314 (3.0 x 10^4), 422 (1.0 x 10^4), 519 (6.8 x 10^3). HRMS (ESI): Calcd *m/z* for **3**-2PF_6: 668.1111; Found: 668.1145

Synthesis of [(μ-PPP)Co(NCMe)]$_2$[PF$_6$]$_2$ (4). Complex **3** (38 mg, 0.024 mmol) was dissolved in THF (5 mL). To a stirring solution of **3**, MeCN (2.7 µL, 0.050 mmol) was added via micropipette. The solution immediately turned purple and was stirred at room temperature for 30 min. The solution was then filtered through Celite and the solvent was removed from the filtrate in vacuo. The resulting purple solid was washed with hexanes and dried, yielding **4** as a solid (35 mg, 85%). Crystals of **4** suitable for X-ray diffraction were grown by layering Et_2O onto a concentrated CH_2Cl_2 solution of **4**. ^{1}H NMR (400 MHz, CD_2Cl_2): δ 7.56 (br s, Ar-H, 2H), 7.44 (br m, Ar-H, 2H), 7.40 (br m, Ar-H, 8H), 7.31 (br m, Ar-H, 4H), 7.21 (br s, Ar-H, 8H), 7.14 (br m, Ar-H, 4H), 7.02 (br m, Ar-H, 8H), 6.97 (br m, Ar-H, 6H), 6.80 (t, Ar-H, 2H), 6.67 (t, Ar-H, 2H), 6.61 (t, Ar-H, 2H), 6.52 (br s, Ar-H, 4H), 6.27 (br s, Ar-H, 2H), 5.78 (br m, Ar-H, 2H), 4.28 (br m, CH_2, 2H), 3.75 (br m, CH_2, 4H), 3.67 (br m, CH_2, 2H), 0.62 (s, MeCN, 6H). ^{31}P{^{1}H} (161.8 MHz, CD_2Cl_2): δ 215.5 (m, P^{NHP}, 2P), 43.1 (s, PPh_2, 2P), 20.0 (m, PPh_2, 2P), -143.4 (septet, $J_{P\text{-}F}$ = 711 Hz, PF_6, 2P). ^{19}F NMR (376 MHz, CD_2Cl_2): δ -73.0 (d, $J_{F\text{-}P}$ = 711 Hz, PF_6, 12 F). ^{13}C{^{1}H} NMR (100.5 MHz, CD_2Cl_2): δ 151.5 (s), 150.2 (s), 135.8 (s), 134.5 (s), 134.1 (s), 133.5 (s), 132.2 (s), 131.6 (s), 131.5 (s), 131.3 (s), 131.1 (s), 130.7 (s), 130.5 (br s), 129.5 (br s), 128.9 (s), 128.8 (s), 125.7 (s), 124.8 (s), 124.0 (s), 118.6 (s), 55.3 (s, CH_2), 48.8 (s, CH_2), 4.5 (s, MeCN). UV-Vis (THF, λ(nm) (ε, $M^{-1}cm^{-1}$): 321 (2.3 x 10^4), 548 (4.2 x 10^3). HRMS (ESI): Calcd *m/z* for **4**-2PF_6-2MeCN: 668.1111; Found: 668.1145.

Synthesis of [(μ-PPP)Co]$_2$][PF$_6$] (5^X). Route 1 to 5^{PF6}: Complex **2** (23 mg, 0.017 mmol) was dissolved in THF (4 mL). $FcPF_6$ (59 mg, 0.018 mmol) was dissolved in THF (2 mL) and added to the stirring solution of **2**. The resulting solution was allowed to stir at room temperature for 16 hours. The solution was then filtered through Celite and the solvent was removed from the filtrate in vacuo. The remaining solid was washed with Et_2O (3 x 3 mL) and extracted with THF (5 mL) and filtered through Celite once more. The solvent was removed from the THF extracts in vacuo, yielding $\mathbf{5^{PF6}}$ as a yellow/brown oily residue (18 mg, 78 %). **Route 2 to 5^{PF6}:** Complex **2** (35 mg, 0.026 mmol) and complex **3** (43 mg, 0.026 mmol) were each dissolved in THF (2 mL). The solution of complex **2** was added to the stirring solution of **3** and the mixture was allowed to stir for 16 hours. The resulting dark yellow/brown solution was filtered through Celite and the solvent was removed from the filtrate in vacuo. The resulting oil was washed with Et_2O (3 x 3 mL) and the solid was collected and dried in vacuo, yielding $\mathbf{5^{PF6}}$ as a solid (26 mg, 68 %). **Route 3 to 5^{BPh4} via 5^{Cl}**: Complex **2** (18.8 mg, 0.014 mmol) was dissolved in CH_2Cl_2 (10 mL) and stirred at room temperature for 16 h. The red/brown solution was filtered and volatile components were removed in vacuo yielding $\mathbf{5^{Cl}}$ as a red/brown solid (17 mg, 89%). Complex $\mathbf{5^{Cl}}$ (15.5 mg, 0.011 mmol) was then dissolved in CH_2Cl_2 (5 mL). $NaBPh_4$ suspended in CH_2Cl_2 (2 mL) was added to the stirring solution of $\mathbf{5^{Cl}}$ and was stirred for 2 hours at room temperature. The red/brown solution was filtered through Celite and volatiles were removed from the filtrate in vacuo yielding $\mathbf{5^{BPh4}}$ as a red/brown solid (17.2 mg, 91%). Crystals of $\mathbf{5^{BPh4}}$ suitable for X-ray diffraction were grown via layering diethyl ether onto a concentrated CH_2Cl_2 solution of $\mathbf{5^{BPh4}}$. $\mathbf{5^{PF6}}$: ^{1}H NMR (400 MHz, CD_2Cl_2): δ 18.61 (br s), 8.14 (br s) 7.94 (br s), 6.86 (br s), 6.65-6.39 (br s two overlapping signals), 4.27 (br s). ^{31}P{^{1}H} (161.8 MHz, CD_2Cl_2): δ -143.6 (septet, PF_6, $J_{P\text{-}F}$ = 709 Hz). ^{19}F NMR (376 MHz, CD_2Cl_2): δ -72.6 (PF_6, $J_{P\text{-}F}$ = 709 Hz). $\mathbf{5^{BPh4}}$: ^{1}H NMR (400 MHz, CD_2Cl_2): δ 18.92 (br s), 8.10 (br s) 7.88 (br s), 7.34 (br, s), 7.04 (br, s, BPh_4), 6.89 (br, two overlapping signals, BPh_4), 6.59 (br, s), 6.49 (br s), 4.38 (br s). ^{11}B NMR (64.74 MHz, CD_2Cl_2): δ -6.84. $\mathbf{5^{Cl}}$: ^{1}H NMR (400 MHz, CD_2Cl_2): δ 19.08 (br, s), 8.20 (br, s), 7.99 (br, s), 6.84 (br, s), 6.52 (br, s), 6.44 (br, s), 4.15 (br, s). UV-Vis (THF, λ(nm) (ε, $M^{-1}cm^{-1}$): 351 (sh), 405 (sh), 544 (2.5 x 10^3). HRMS (ESI):. Calcd *m/z* for $\mathbf{5^{Cl}}$: 1372.1911; Found: 1372.1909. Evans' Method solution state magnetic moment of $\mathbf{5^{Cl}}$ in CD_2Cl_2: μ_{eff} = 1.68 μ_B.

Synthesis of [(PPP)CoCl]$_2$ (6): Complex **1** (32 mg, 0.042 mmol) was suspended in THF (5 mL) and placed in a glovebox cold well cooled with liquid N_2 until frozen. Cp_2Co (16 mg, 0.086 mmol) was dissolved in THF (5 mL) and frozen. Upon thawing, the Cp_2Co solution was added to the frozen suspension of **1**. The reaction was warmed to room temperature and stirred for 1 hour. The resulting dark green solution was filtered through Celite and the solvent was removed from the filtrate in vacuo. The resulting crude green oil was washed with Et_2O (3 x 5 mL) and the solid was collected and dried in vacuo. The green solid was dissolved in benzene and filtered through Celite and the solvent was removed from the filtrate in vacuo, affording **6** as a green powder. (22 mg, 75%). Crystals of **6** suitable for X-ray diffraction were grown via vapor diffusion of pentane into a concentrated toluene solution of **6**. ^{1}H NMR (600 MHz, C_6D_6): δ 8.06 (s, Ar-H, 4H), 7.56 (br s, Ar-H, 4H), 7.48 (br m, Ar-H, 4H), 7.43 (br s, Ar-H, 4H), 7.35 (s, Ar-H, 10H), 7.06, (s, Ar-H, 2H), 6.93 (s, Ar-H, 4H), 6.83 (br m, Ar-H, 2H) 6.79 (br m, Ar-H, 4H), 6.48-6.58 (br overlapping signals, Ar-H, 10H), 6.46 (br m, Ar-H 4H), 6.32 (br m, Ar-H, 2H), 6.29 (br m, Ar-H, 2H) 3.91 (br m, CH_2, 2H), 3.74 (br m, CH_2, 2H), 3.25 (br m, CH_2, 2H), 2.77 (br m, CH_2, 2H). ^{31}P{^{1}H} NMR (242.8 MHz, C_6D_6): δ 218.7 (d, $J_{P\text{-}P}$ = 160 Hz, NHP, 2P), 40.6 (s, PPh_2, 2P), 16.7 (d, $J_{P\text{-}P}$ = 160 Hz, 2P). ^{13}C{^{1}H} NMR (150.8 MHz, C_6D_6): δ 150.9 (s), 150.6 (s), 138.3 (s), 138.3-137.9 (br overlapping signals), 135.1 (s), 134.7 (s), 133.4-133.6 (two overlapping signals), 132.1 (s), 131.2 (s), 131.1 (s), 130.8 (s), 128.7 (br s), 128.6 (s), 128.3 (s overlapping with solvent), 127.7-127.5 (two overlapping signals), 127.1 (s), 126.7-126.8 (two overlapping signals), 124.3 (s), 122.3 (s), 121.3 (s), 120.7 (s), 117.7 (s), 50.7 (s, CH_2), 47.1 (s, CH_2). UV-Vis (THF, λ(nm) (ε, $M^{-1}cm^{-1}$): 310 (sh), 371 (1.3 x 10^4), 444

(sh), 594 (1.8 x 10^3), 751 (1.4 x 10^3). HRMS (ESI): Calcd *m/z* for **6**: 1406.1598; Found: 1406.1600.

Synthesis of [(PPP)CoH]$_2$ (7): Complex **1** (29 mg, 0.037 mmol) was suspended in THF (5 mL) and was placed in a glovebox cold well cooled by liquid N_2 until frozen. Upon thawing of the solution of **1**, $KBEt_3H$ (1 M in THF, 114 µL, 0.114 mmol) was added directly to the stirring solution. The solution immediately turned dark red and became homogenous. The resulting red solution was stirred for 20 minutes at room temperature. The dark red solution was filtered through Celite and the solvent was removed from the filtrate in vacuo. The crude red solid was dissolved in dioxane and filtered through Celite and solvent was removed from the filtrate in vacuo yielding **7** as a pure solid (23 mg, 90 %). Crystals of **7** suitable for X-ray diffraction were grown via vapor diffusion of hexanes into a concentrated solution of **7** in dioxane. Complex **7** co-crystalizes with three dioxane solvent molecules per metal complex. Excess manipulation of **7** to remove the dioxane solvate results in degradation to complex **2**. ^{1}H NMR (400 MHz, C_6D_6): δ 7.51 (s, Ar-H, 8H), 7.22-7.11 (overlapping with solvent peak, 8H), 6.86-7.06 (br m, Ar-H, 20H), 6.51-6.61 (br m, Ar-H, 16H), 6.44 (t, $J_{H\text{-}P}$ = 7.1 Hz, Ar-H, 4H), 3.69 (s, CH_2, 4H), 3.29 (s, CH_2, 4H), -8.28 (br s, Co-H, 2H). ^{31}P{^{1}H} NMR (161.8 MHz, C_6D_6): δ 289.6 (br s, NHP, 2P), 45.6 (br s, PPh_2, 4P). ^{13}C{^{1}H} NMR (100.5 MHz, C_6D_6): δ 134.8 (s), 134.1 (s), 133.1 (s). 129.4 (s), 128.5 (s), 128.4 (s), 127.6 (s),127.1 (s), 126.9 (s), 126.7 (s), 119.4 (s), 119.1 (s), 47.1 (s, CH_2). UV-Vis (THF, λ(nm) (ε, $M^{-1}cm^{-1}$): 306 (1.7 x 10^4), 374 (1.0 x 10^4), 529 (2.8 x 10^3), 870 (br, 600). HRMS (ESI): Calcd *m/z* for **7**+MeCN: 1379.2643; Found: 1379.2636.

Electrochemistry. Cyclic voltammetry measurements were carried out in a glovebox under a dinitrogen atmosphere in a one-compartment cell using a CH Instruments 620E electrochemical analyzer. A glassy carbon electrode, platinum wire, and $Ag/AgNO_3$ non-aqueous electrode were used as the working, auxiliary, and reference electrodes, respectively. Solutions (THF) of electrolyte (0.3 M [^{n}Bu$_4$N][PF_6]) and analyte were also prepared in the glovebox. All potentials are reported versus the Fc/Fc^+ couple by comparison to an internal ferrocene reference added following data collection.

EPR Spectroscopy. The X-Band EPR spectrum of $\mathbf{5^{Cl}}$ was obtained using a Bruker EMXPlus Electron Paramagnetic Resonance Spectrometer fitted with a Cold-Edge cryogen-free helium-recycling cryostat for measurements at 4 K. Complex $\mathbf{5^{Cl}}$ was generated using the procedure described above (Route 3) without the anion exchange step and the sample was prepared via dissolution of $\mathbf{5^{Cl}}$ in dry, degassed THF to make an approximately 1 mM solution, followed by filtration to ensure homogeneity. The spectrum was simulated using EasySpin for MATLAB.[23]

X-ray crystallography. Crystals of complex **2**-**7** were coated with paratone and mounted on a MiTeGen loop. All operations were performed on either a Bruker-Nonius Kappa Apex2 diffractometer (**2**, **6**) or a Bruker D8 Venture PHOTON II CPAD system (**3**, **4**, $\mathbf{5^{BPh4}}$, **7**) using graphite-monochromated Mo Kα radiation. All diffractometer manipulations, including data collection, integration, scaling, and absorption corrections were carried out using the Bruker Apex2 (**2**)[24] or Apex3 (**3**-**7**)[25] software. Further crystallographic data collection, solution, and refinement details are available on pages S22-S29 of the Supporting Information file or in the accompanying .cif files.

Computational Details. All calculations were performed using Gaussian16 for Linux operating system.[26] DFT calculations were carried out using M06 functional.[27] A mixed basis set was employed using the LANL2DZ(*p*, *d*) double-ζ basis set with effective core potentials for the P, Cl, and Co atoms[28] and Gaussian09's internal LANL2DZ basis set (equivalent to D95V[29]) for C, N, and H atoms. Additional details about how the appropriate functional and basis set were chosen are included on pages S30-S32 of the Supporting Information file. Starting from crystallographically determined coordinates, the geometries of **2**, **3**, and **5** were optimized to a minimum. The optimized geometry of **5'** was obtained by starting a DFT geometry optimization from the crystallographic coordinates of **2**. The optimized geometries of $\mathbf{6^{monomer}}$ and $\mathbf{7^{monomer}}$ were obtained by starting a DFT geometry optimization from the crystallographic coordinates of half of **6** and **7**. Analytical frequency calculations were used to confirm that no imaginary frequencies were present. Single point NBO calculations were subsequently performed using NBO3.1,[30] as implemented in Gaussian16. Mayer bond order (MBO) analysis was performed using routines included in the Gaussian16 package.[31] Further computational details and a table of XYZ coordinates of all calculated compounds are provided on pages S26-S57 of the Supporting Information file.

ASSOCIATED CONTENT

Supporting Information

The Supporting Information is available free of charge on the ACS Publications website.

NMR data (^{1}H, ^{31}P, ^{19}F, ^{13}C, ^{11}B) for complexes **2**-**7**, UV-Vis spectra of **2**-**7**, cyclic voltammetry data for (PPP)$CoPMe_3$, crystallographic data collection and refinement details for **2**-**7**, additional computational details and XYZ coordinates of DFT-optimized geometries for **2**, **3**, **5**, **5'**, $\mathbf{6^{monomer}}$ and $\mathbf{7^{monomer}}$ (PDF)

Accession Codes

CCDC 1974215-1974219 and 1974221 (compounds **2**-**7**) contain the supplementary crystallographic data for this paper. These data can be obtained free of charge via www.ccdc.cam.ac.uk/data_request/cif, or by emailing

data_ request@ccdc.cam.ac.uk, or by contacting The Cambridge Crystallographic Data Centre, 12 Union Road, Cambridge CB2 1EZ, UK; fax: +44 1223 336033.

AUTHOR INFORMATION

Corresponding Author

E-mail: thomasc@chemistry.ohio-state.edu

Present Addresses

[§]D. A. Dickie, Department of Chemistry, University of Virginia, Charlottesville, VA 22904, United States.

ACKNOWLEDGMENT

This material is based upon work supported by the National Science Foundation under award number CHE-1764170. The Ohio State University Department of Chemistry and Biochemistry and The Ohio State Sustainability Institute are also gratefully acknowledged for financial support. All computational studies were performed using resources provided by the Ohio Supercomputer Center.[32]

REFERENCES

1. (a) Fleming, S.; Lupton, M. K.; Jekot, K. Synthesis of a Cyclic Fluorodialkylaminophosphine and its Coordination with Boron Acids. Formation of a Unique Dialkylaminophosphine Cation. *Inorg. Chem.* **1972**, *11*, 2534-2540; (b) Gudat, D. Cationic Low Coordinated Phosphorus Compounds as Ligands: Recent Developments. *Coord. Chem. Rev.* **1997**, *163*, 71-106; (c) Gudat, D. Cation Stabilities, Electrophilicities, and "Carbene Analogue" Character of Low Coordinate Phosphorus Cations. *Eur. J. Inorg. Chem.* **1998**, *1998*, 1087-1094; (d) Gudat, D.; Haghverdi, A.; Hupfer, H.; Nieger, M. Stability and Electrophilicity of Phosphorus Analogues of Arduengo Carbenes—An Experimental and Computational Study. *Chem. Eur. J.* **2000**, *6*, 3414-3425; (e) Cowley, A. H.; Kemp, R. A. Synthesis and Reaction Chemistry of Stable Two-Coordinate Phosphorus Cations (Phosphenium Ions). *Chem. Rev.* **1985**, *85*, 367-382; (f) Rosenberg, L. Metal Complexes of Planar PR_2 Ligands: Examining the Carbene Analogy. *Coord. Chem. Rev.* **2012**, *256*, 606-626; (g) Lundrigan, T.; Welsh, E. N.; Hynes, T.; Tien, C.-H.; Adams, M. R.; Roy, K. R.; Robertson, K. N.; Speed, A. W. H. Enantioselective Imine Reduction Catalyzed by Phosphenium Ions. *J. Am. Chem. Soc.* **2019**, *141*, 14083-14088.

2. (a) Hutchins, L. D.; Duesler, E. N.; Paine, R. T. Structure and Bonding in a Phosphenium Ion-Iron complex, $Fe[\eta^5\text{-}(CH_3)_5C_5](CO)_2[PN(CH_3)CH_2CH_2NCH_3]$. A Demonstration of Phosphenium Ion Acceptor Properties. *Organometallics* **1982**, *1*, 1254-1256; (b) Nickolaus, J.; Schlindwein, S. H.; Nieger, M.; Gudat, D. N-Heterocyclic Phosphenium Dihalido-Aurates: On the Borderline between Classical Coordination Compounds and Ion Pairs. *Z. Anorg. Allg. Chem.* **2017**, *643*, 1849-1854; (c) Nickolaus, J.; Imbrich, D. A.; Schlindwein, S. H.; Geyer, A. H.; Nieger, M.; Gudat, D. Phosphenium Hydride Reduction of $[(cod)MX_2]$ (M = Pd, Pt; X = Cl, Br): Snapshots on the Way to Phosphenium Metal(0) Halides and Synthesis of Metal Nanoparticles. *Inorg. Chem.* **2017**, *56*, 3071-3080.

3. (a) Caputo, C. A.; Brazeau, A. L.; Hynes, Z.; Price, J. T.; Tuononen, H. M.; Jones, N. D. A Cation-Captured Palladium(0) Anion: Synthesis, Structure, and Bonding of $[PdBr(PPh_3)_2]^-$ Ligated by an N-Heterocyclic Phosphenium Cation. *Organometallics* **2009**, *28*, 5261-5265; (b) Pan, B.; Xu, Z.; Bezpalko, M. W.; Foxman, B. M.; Thomas, C. M. N-Heterocyclic Phosphenium Ligands as Sterically and Electronically-Tunable Isolobal Analogues of Nitrosyls. *Inorg. Chem.* **2012**, *51*, 4170-4179; (c) Hamilton, C. W.; Morris, D. E.; Blair, M. W.; Jenson, N. J.; Martin, R. L.; Cross, J. L.; Sutton, A. D.; Jantunen, K. C.; Scott, B. L.; Baker, R. T. In *INOR 50-When is addition of X-Y to M not oxidative?*, 235th American Chemical Society National Meeting, New Orleans, LA, New Orleans, LA, 2008; (d) Feil, C. M.; Hettich, T. D.; Beyer, K.; Sondermann, C.; Schlindwein, S. H.; Nieger, M.; Gudat, D. Comparing the Ligand Behavior of N-Heterocyclic Phosphenium and Nitrosyl Units in Iron and Chromium Complexes. *Inorg. Chem.* **2019**, *58*, 6517-6528.

4. Day, G. S.; Pan, B.; Kellenberger, D. L.; Foxman, B. M.; Thomas, C. M. Guilty as Charged: Non-Innocent Behavior by a Pincer Ligand Featuring a Central Cationic Phosphenium Donor. *Chem. Commun.* **2011**, *47*, 3634-3636.

5. (a) Poitras, A. M.; Knight, S. E.; Bezpalko, M. W.; Foxman, B. M.; Thomas, C. M. Addition of H_2 Across a Cobalt–Phosphorus Bond. *Angew. Chem. Int. Ed.* **2018**, *57*, 1497-1500; (b) Evers-McGregor, D. A.; Bezpalko, M.

W.; Foxman, B. M.; Thomas, C. M. N-Heterocyclic Phosphenium and Phosphido Nickel Complexes Supported by a Pincer Ligand Framework. *Dalton Trans.* **2016**, *45*, 1918-1929; (c) Pan, B.; Bezpalko, M. W.; Foxman, B. M.; Thomas, C. M. Coordination of an N-Heterocyclic Phosphenium Containing Pincer Ligand to a $Co(CO)_2$ Fragment Allows Oxidation To Form an Unusual N-Heterocyclic Phosphinito Species. *Organometallics* **2011**, *30*, 5560-5563.
6. (a) Bezpalko, M. W.; Poitras, A. M.; Foxman, B. M.; Thomas, C. M. Cobalt N-Heterocyclic Phosphenium Complexes Stabilized by a Chelating Framework: Synthesis and Redox Properties. *Inorg. Chem.* **2017**, *56*, 503-510; (b) Bezpalko, M. W.; Foxman, B. M.; Thomas, C. M. Use of a Bidentate Ligand Featuring an N-Heterocyclic Phosphenium Cation (NHP^+) to Systematically Explore the Bonding of NHP^+ Ligands with Nickel. *Inorg. Chem.* **2015**, *54*, 8717-8726; (c) Caputo, C. A.; Jennings, M. C.; Tuononen, H. M.; Jones, N. D. Phospha-Fischer Carbenes: Synthesis, Structure, Bonding, and Reactions of Pd(0)- and Pt(0)-Phosphenium Complexes. *Organometallics* **2009**, *28*, 990-1000; (d) Burck, S.; Daniels, J.; Gans-Eichler, T.; Gudat, D.; Nättinen, K.; Nieger, M. N-Heterocyclic Phosphenium, Arsenium, and Stibenium Ions as Ligands in Transition Metal Complexes: A Comparative Experimental and Computational Study. *Z. Anorg. Allg. Chem.* **2005**, *631*, 1403-1412.
7. Pan, B.; Evers-McGregor, D. A.; Bezpalko, M. W.; Foxman, B. M.; Thomas, C. M. Multimetallic Complexes Featuring a Bridging N-heterocyclic Phosphido/Phosphenium Ligand: Synthesis, Structure, and Theoretical Investigation. *Inorg. Chem.* **2013**, *52*, 9583-9589.
8. Hutchins, L. D.; Light, R. W.; Paine, R. T. Synthesis, Structure, and Bonding of the Bis(phosphenium) Ion-Dicobalt Carbonyl Complex $Co_2(CO)_5(\mu\text{-}PN(CH_3)CH_2CH_2NCH_3)_2$. *Inorg. Chem.* **1982**, *21*, 266-272.
9. Förster, D.; Nickolaus, J.; Nieger, M.; Benkõ, Z.; Ehlers, A. W.; Gudat, D. Donor-Free Phosphenium-Metal(0)-Halides with Unsymmetrically Bridging Phosphenium Ligands. *Inorg. Chem.* **2013**, *52*, 7699-7708.
10. Kim, Y.-E.; Lee, Y. A P−P Bond as a Redox Reservoir and an Active Reaction Site. *Angew. Chem. Int. Ed.* **2018**, *57*, 14159-14163.
11. (a) Harkins, S. B.; Mankad, N. P.; Miller, A. J. M.; Szilagyi, R. K.; Peters, J. C. Probing the Electronic Structures of $[Cu_2(\mu\text{-}XR_2)]^{n+}$ Diamond Cores as a Function of the Bridging X Atom (X = N or P) and Charge (n = 0, 1, 2). *J. Am. Chem. Soc.* **2008**, *130*, 3478-3485; (b) Mankad, N. P.; Harkins, S. B.; Antholine, W. E.; Peters, J. C. Multifrequency EPR Studies of $[Cu^{1.5}Cu^{1.5}]^+$ for $Cu_2(\mu\text{-}NR_2)_2$ and $Cu_2(\mu\text{-}PR_2)_2$ Diamond Cores. *Inorg. Chem.* **2009**, *48*, 7026-7032.
12. Poitras, A. M.; Bezpalko, M. W.; Foxman, B. M.; Thomas, C. M. Cooperative Activation of O–H and S–H Bonds Across the Co–P Bond of an N-Heterocyclic Phosphido Complex. *Dalton Trans.* **2019**, *48*, 3074-3079.
13. Oxidation of **B** with $FcPF_6$ leads to appreciable formation of the mixed valence complex $\mathbf{5^{PF6}}$.
14. (a) Sur, S. K. Measurement of Magnetic Susceptibility and Magnetic Moment of Paramagnetic Molecules in Solution by high-field Fourier-Transform NMR Spectroscopy. *J. Magn. Reson.* **1989**, *82*, 169-173; (b) Evans, D. F. The Determination of the Paramagnetic Susceptibility of Substances in Solution by Nuclear Magnetic Resonance. *J. Chem. Soc.* **1959**, 2003-2005.
15. The broad features of the EPR signal likely result from additional smaller hyperfine interactions with the sec-ond ^{59}Co center and the ^{31}P ($I = ½$) nuclei. Additional hyperfine coupling constants cannot be unambiguously assigned and were instead modeled using Gaussian line broadening of 7 mT (peak-to-peak) and anistotropic residual line width (HStrain) for the g tensor centered at 2.27 (500 MHz).
16. (a) Und, E. K.; Vahrenkamp, H. Stereochemie der Metall-Metall-Bindung. Die Strukturen dreier Komplexe des Typs $[L_2M\text{-}PR_2]_2$. *Chem. Ber.* **1979**, *112*, 1626-1634; (b) Jones, R. A.; Stuart, A. L.; Atwood, J. L.; Hunter, W. E.; Rogers, R. D. Steric Effects of Phosphido Ligands. Synthesis and Crystal Structures of Bis(*tert*-butylphosphido)-Bridged Dinuclear Metal-Metal-Bonded Complexes of Iron(II), Cobalt(I, II) and Nickel(I). *Organometallics* **1982**, *1*, 1721-1723; (c) Jones, R. A.; Stuart, A.

L.; Atwood, J. L.; Hunter, W. E. Synthesis of di-*tert*-butylphosphido-bridged dimers of cobalt(I) containing cobalt-cobalt double bonds. Crystal structures of $[Co\{\mu\text{-}(Me_3C)_2P\}(CO)_2]_2$ and $[Co\{\mu\text{-}(Me_3C)_2P\}(PMe_3)L]_2$ (L = CO or N_2). *Organometallics* **1983**, *2*, 1437-1441; (d) Harley, A. D.; Whittle, R. R.; Geoffroy, G. L. Crystal and Molecular Structure of Binuclear $Co_2(\mu\text{-}PPh_2)_2(CO)_2(PEt_2Ph)_2$, a Phosphido-Bridged Compound with a Formal Cobalt-Cobalt Double Bond. *Organometallics* **1983**, *2*, 60-63; (e) Harley, A. D.; Whittle, R. R.; Geoffroy, G. L. Crystal and Molecular Structures of Bent and Planar Forms of Binuclear $Co_2(\mu\text{-}PPh_2)_2(CO)_6$ (**1**). Comments on the Relative Energies of the Two Forms of **1** and Related Molecules. *Organometallics* **1983**, *2*, 383-387; (f) Werner, H.; Hofmann, W.; Zolk, R.; Dahl, L. F.; Kocal, J.; Kühn, A. Synthesis and Reactions of a Nucleophilic Bis(μ-dimethylphosphido)dicobalt Complex. The Crystal and Molecular Structure of $[C_5H_5Co(\mu\text{-}PMe_2)]_2$ and $[(C_5H_5Co)_2(\mu\text{-}H)(\mu\text{-}PMe_2)_2]BPh_4$. *J. Organomet. Chem.* **1985**, *289*, 173-188; (g) Chen, L.; Kountz, D. J.; Meek, D. W. New Bimetallic Cobalt(II) Complexes of Chelated, Bridged Phosphido Ligands. *Organometallics* **1985**, *4*, 598-601; (h) Geoffroy, G. L.; Mercer, W. C.; Whittle, R. R.; Marko, L.; Vastag, S. Further Examples of (Diphenylphosphido)-Bridged Dicobalt Complexes: $Co_2(\mu\text{-}PPh_2)_2(CO)_4(PPh_2H)_2$ and $Co_2(\mu\text{-}PPh_2)_2(CO)_2(PPh_2H)_2$. *Inorg. Chem.* **1985**, *24*, 3771-3774; (i) Klein, H.-F.; Gaß, M.; Zucha, U.; Eisenmann, B. Di(μ-phosphido)cobalt Und Nickel-Verbindungen mit Trimethylphosphanliganden/ Di(μ-phosphido)cobalt and Nickel Compounds with Trimethylphosphine Ligands. *Z. Naturforsch., B: Chem. Sci.* **1988**, *43*, 927; (j) Lang, H.; Eberle, U.; Leise, M.; Zsolnai, L. Synthese und Reaktionsverhalten von $(R)(\eta^1\text{-}C_5Me_5)P{=}Co(CO)_3$. *J. Organomet. Chem.* **1996**, *519*, 137-145; (k) Winterhalter, U.; Zsolnai, L.; Kircher, P.; Heinze, K.; Huttner, G. Reductive Activation of Tripod Cobalt Compounds: Oxidative Addition of H−H, P−H, and Sn−H Functions. *Eur. J. Inorg. Chem.* **2001**, *2001*, 89-103; (l) Kornev, A. N.; Sushev, V. V.; Panova, Y. S.; Belina, N. V.; Lukoyanova, O. V.; Fukin, G. K.; Ketkov, S. Y.; Abakumov, G. A.; Lönnecke, P.; Hey-Hawkins, E. The Intramolecular Rearrangement of Phosphinohydrazides $[R'_2P\text{–}NR\text{–}NR\text{–}M] \rightarrow [RN{=}PR'_2\text{–}NR\text{–}M]$: General Rules and Exceptions. Transformations of Bulky Phosphinohydrazines $(R\text{–}NH\text{–}N(PPh_2)_2$, R = ^{t}Bu, Ph_2P). *Inorg. Chem.* **2012**, *51*, 874-881; (m) Beck, R.; Klein, H.-F. Bis(μ-diphenylphosphanyl)bis[(trimethylphosphane)cobalt(I)](Co-Co). *Acta Crystallographica Section E* **2013**, *69*, m604.

17. The ratio of the Co-Co distance to the sum of the Pauling single bond atomic radii (R_1) of two Co centers is 1.03.

18. Fout, A. R.; Basuli, F.; Fan, H.; Tomaszewski, J.; Huffman, J. C.; Baik, M.-H.; Mindiola, D. J. A Co_2N_2 Diamond-Core Resting State of Cobalt(I): A Three-Coordinate Co^I Synthon Invoking an Unusual Pincer-Type Rearrangement. *Angew. Chem. Int. Ed.* **2006**, *45*, 3291-3295.

19. Rozenel, S. S.; Padilla, R.; Arnold, J. Chemistry of Reduced Monomeric and Dimeric Cobalt Complexes Supported by a PNP Pincer Ligand. *Inorg. Chem.* **2013**, *52*, 11544-11550.

20. The ratio of the Co-Co distance to the sum of the Pauling single bond atomic radii (R_1) of two Co centers is 1.06.

21. The ratio of the Co-Co distance to the sum of the Pauling single bond atomic radii (R_1) of two Co centers is 1.08.

22. Yang, L.; Powell, D. R.; Houser, R. P. Structural variation in copper(i) complexes with pyridylmethylamide ligands: structural analysis with a new four-coordinate geometry index, [small tau]4. *Dalton Trans.* **2007**, 955-964.

23. Stoll, S.; Schweiger, A. EasySpin, a comprehensive software package for spectral simulation and analysis in EPR. *J. Magn. Reson.* **2006**, *178*, 42-55.

24. *Apex 2: Version 2 User Manual, M86-E01078*. Bruker Analytical X-ray Systems: Madison, WI, 2006.

25. Bruker *Saint; SADABS; APEX3.*, Bruker AXS Inc.: Madison, Wisconsin, USA, 2012.

26. Frisch, M. J.; Trucks, G. W.; Schlegel, H. B.; Scuseria, G. E.; Robb, M. A.; Cheeseman, J. R.; Scalmani, G.; Barone, V.; Petersson, G. A.; Nakatsuji, H.; Li, X.; Caricato, M.; Marenich, A.

V.; Bloino, J.; Janesko, B. G.; Gomperts, R.; Mennucci, B.; Hratchian, H. P.; Ortiz, J. V.; Izmaylov, A. F.; Sonnenberg, J. L.; Williams; Ding, F.; Lipparini, F.; Egidi, F.; Goings, J.; Peng, B.; Petrone, A.; Henderson, T.; Ranasinghe, D.; Zakrzewski, V. G.; Gao, J.; Rega, N.; Zheng, G.; Liang, W.; Hada, M.; Ehara, M.; Toyota, K.; Fukuda, R.; Hasegawa, J.; Ishida, M.; Nakajima, T.; Honda, Y.; Kitao, O.; Nakai, H.; Vreven, T.; Throssell, K.; Montgomery Jr., J. A.; Peralta, J. E.; Ogliaro, F.; Bearpark, M. J.; Heyd, J. J.; Brothers, E. N.; Kudin, K. N.; Staroverov, V. N.; Keith, T. A.; Kobayashi, R.; Normand, J.; Raghavachari, K.; Rendell, A. P.; Burant, J. C.; Iyengar, S. S.; Tomasi, J.; Cossi, M.; Millam, J. M.; Klene, M.; Adamo, C.; Cammi, R.; Ochterski, J. W.; Martin, R. L.; Morokuma, K.; Farkas, O.; Foresman, J. B.; Fox, D. J. *Gaussian 16 Rev. C.01*, Wallingford, CT, 2016.

27. Zhao, Y.; Truhlar, D. G. The M06 suite of density functionals for main group thermochemistry, thermochemical kinetics, noncovalent interactions, excited states, and transition elements: two new functionals and systematic testing of four M06-class functionals and 12 other functionals. *Theor. Chem. Acc.* **2008**, *120*, 215-241.

28. (a) Hay, P. J.; Wadt, W. R. *Ab Initio* Effective Core Potentials for Molecular Calculations - Potentials for the Transition-Metal Atoms Sc To Hg. *J. Chem. Phys.* **1985**, *82*, 270-283; (b) Hay, P. J.; Wadt, W. R. *Ab Initio* Effective Core Potentials for Molecular Calculations - Potentials for K to Au Including the Outermost Core Orbitals. *J. Chem. Phys.* **1985**, *82*, 299-310; (c) Hay, P. J.; Wadt, W. R. Ab Initio Effective Core Potentials for Molecular Calculations. Potentials for Main Group Elements Na to Bi. *J. Chem. Phys.* **1985**, *82*, 284-298; (d) Roy, L. E.; Hay, P. J.; Martin, R. L. Revised Basis Sets for the LANL Effective Core Potentials. *J. Chem. Theory Comput.* **2008**, *4*, 1029-1031.

29. Dunning, T. H., Hay, P. J., in: H.F. Schaefer (Ed.), Modern Theoretical Chemistry, Plenum, New York, 1976, pp. 1–28.

30. Glendening, E. D.; Reed, A. E.; Carpenter, J. E.; Weinhold, F. *NBO Version 3.1*.

31. Mayer, I. Bond Orders and Valences from ab-initio Wave-Functions. *Int. J. Quantum Chem* **1986**, *29*, 477-483.

32. *Ohio Supercomputer Center*. Columbus, OH, 1987.

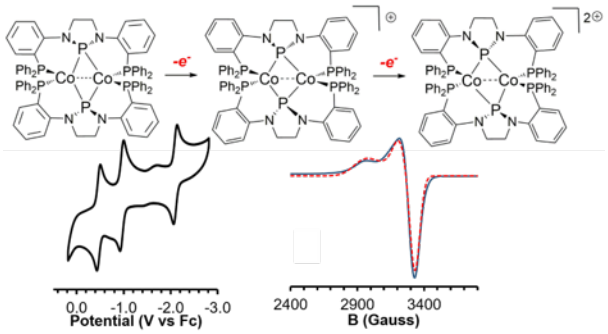

A family of *N*-heterocyclic phosphido-bridged dicobalt complexes have been synthesized and structurally characterized. Substantial structural reorganization is observed as a function of redox processes, suggesting that both phosphorus and cobalt participate in redox processes.